NANO LETTERS

Letter

pubs.acs.org/NanoLett

Probing the Structure, Composition, and Spatial Distribution of Ligands on Gold Nanorods

Michael J. A. Hore,*[,†,‡] Xingchen Ye,[§] Jamie Ford,[∥] Yuzhi Gao,[⊥] Jiayang Fei,[⊥] Qiong Wu,[‡] Stuart J. Rowan,[‡] Russell J. Composto,[⊥] Christopher B. Murray,[§,⊥] and Boualem Hammouda[†]

[†]National Institute of Standards and Technology, Center for Neutron Research, 100 Bureau Drive, Gaithersburg, Maryland 20899, United States

[‡]Department of Macromolecular Science & Engineering, Case Western Reserve University, 10900 Euclid Avenue, Cleveland, Ohio 44106, United States

[§]Department of Chemistry, [∥]Nanoscale Characterization Facility, and [⊥]Department of Materials Science & Engineering, University of Pennsylvania, Philadelphia, Pennsylvania 19104, United States

Supporting Information

ABSTRACT: The structure and size of ligands attached to the surfaces of gold nanorods, such as adsorbed surfactants or grafted polymers, are important considerations that facilitate the use of such nanoparticles in the human body, in advanced materials for energy harvesting, or in devices for single molecule detection. Here, we report small-angle neutron scattering (SANS) measurements from surfactant or poly(ethylene glycol) (PEG) coated gold nanorods in solution, which quantitatively determine the location, structure, and composition of these surface layers. In addition, by synthesizing gold nanorods using seed crystals which are coated with deuterated cetyltrimethylammonium bromide (dCTAB), we are able to exploit the isotopic sensitivity of SANS to study, for the first time, the retention of surfactant from the seed crystals to the final gold nanorod product, finding that very little exchange of the deuterated with hydrogenated surfactant occurs. Finally, we demonstrate that, when Au NRs are PEGylated using standard techniques, the surfactant bilayer remains intact, and while mass spectrometry detects the presence of both surfactant and PEG, the composition as measured from SANS is predominantly that of the surfactant. These measurements not only provide new insight into the synthesis and functionalization of gold nanorods but provide a quantitative picture of the structure of grafted polymer and surfactant layers on gold nanorod surfaces which has implications for the fabrication of plasmonic and biomedical materials.

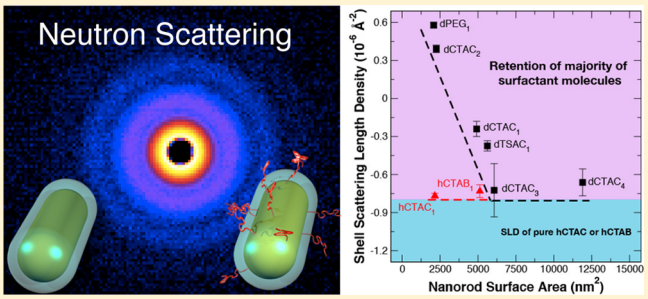

KEYWORDS: *Small-angle neutron scattering, polymer brush, CTAB, CTAC, gold nanorods*

Gold nanorod (Au NR) synthesis has evolved considerably in the past decade,[1] with recent developments leading to lower polydispersities in the size and shape of Au NRs, scaling of the process to large batches (e.g., liter scale), and broadly tunable dimensions through the use of aromatic additives,[2] binary surfactant mixtures,[3] or bromide-free surfactant mixtures.[4] Advances in the synthesis of Au NRs are of great importance for applications that exploit these nanoparticles, as more controlled and refined synthesis schemes lead to materials with well-defined optical responses.

The synthesis of Au NRs is made possible by the preferential adsorption of surfactant molecules, typically cetyltrimethylammonium bromide (CTAB), onto certain facets of seed crystals, thereby leading to anisotropic growth as Au^{+} is reduced to Au. A significant amount of effort has been devoted to understanding the nuances of Au NR synthesis. For instance, Carbó-Argibay and co-workers[5] determined the three-dimensional crystalline structure of Au NRs synthesized with CTAB using high-resolution transmission electron microscopy (HRTEM). Interestingly, this approach reveals the presence of high-index {520} facets, rather than the {110} and {100} facets observed for electrochemically grown Au NRs. A more recent study of the growth mechanism of Au NRs by Park et al.[6] found that the crystalline structure of Au NRs evolves significantly during the growth from seed crystals. When a bromide-free surfactant is used, such as cetyltrimethylammonium chloride (CTAC), {310} facets become the predominant crystalline facets on the NR surface, indicating that the different halide counterions can lead to distinct facetings in the final Au NR products. Thus, one might also ask whether the structure of the CTAC bilayer on the Au NR surface is somehow different from that of a CTAB bilayer. Most recently, Jackson and co-workers

Received: April 21, 2015
Revised: August 18, 2015
Published: August 20, 2015

DOI: 10.1021/acs.nanolett.5b03088
Nano Lett. 2015, 15, 5730−5738

Table 1. Au NR Dimensions, Longitudinal Surface Plasmon Resonance (LSPR) Wavelength, and Theoretical Molar Extinction Coefficients[a]

sample ID	radius R_{NR} (nm)	length L_{NR} (nm)	shell t (nm)	λ_{LSPR} (nm)	ϵ (mol^{-1} L cm^{-1})
$hCTAB_1$	9.9 ± 0.3	82.8 ± 1.5	3.6 ± 0.2	877	4.47×10^9
$hCTAC_1$	10.3 ± 0.1	85.9 ± 1.6	3.0 ± 0.2	1025	4.60×10^9
$hCTAC_2$	13.4 ± 0.1	83.8 ± 3.0	2.39 ± 0.02	688	2.96×10^9
$dCTAC_1$	15.3 ± 0.1	83.4 ± 2.2	2.98 ± 0.02	652	2.12×10^9
$dCTAC_2$	8.34 ± 0.02	42.9 ± 0.2	2.89 ± 0.2	752	3.51×10^9
$dCTAC_3$	15.65 ± 0.02	56.1 ± 0.2	2.38 ± 0.04	657	2.88×10^9
$dCTAC_4$	23.4 ± 0.1	74.5 ± 2.4	2.45 ± 0.05	640	2.11×10^9
$dTSAC_1$	10.7 ± 0.1	59.4 ± 0.3	2.84 ± 0.02	708	3.05×10^9
$dPEG_1$	8.09 ± 0.02	40.7 ± 0.1	3.5 ± 0.2	723	2.68×10^9

[a]The shell thickness $t = t_R = t_L$. Statistical errors correspond to one standard deviation in the least squares fit.

performed energy dispersive X-ray spectroscopy (EDS) studies to determine the location of silver species in Au NRs, finding that it is located along the Au NR surface, and preferentially at crevices near the ends of the NRs.[7] Silver is thought to play a critical role in increasing the yield of Au NRs, relative to other nonrod shapes. Hence, the nature of the surface coating influences the crystalline structure of Au NRs and may further influence the location of silver along the nanorod surface, though this has not yet been investigated to the best of our knowledge.

Following synthesis, Au NRs are often functionalized with thiol-terminated molecules,[8] which increases their solubility in nonaqueous solvents and facilitates their dispersion within polymeric materials.[9] The gold−sulfur bond (approximately 184 kJ mol^{-1})[10] appears to be more energetically favorable compared to desorption of CTAB or CTAC molecules, and facilites functionalization. Both the location and composition of the surface coating on Au NRs are important for their use in biomedical applications or in polymer-based nanocomposites, for example. Vigderman et al.[11] demonstrated using ^{1}H NMR that the CTAB bilayer can be completely replaced by a thiol-terminated CTAB analog, which reduces the cytotoxicity of Au NRs, while increasing their uptake by cancer cells, opening the possibility of using near-infrared (NIR) light to kill the cells. On the other hand, work from the Kumacheva group has shown[12,13] that both the location and composition of the surface coatings are important in the creation of chains of Au NRs in solution, by selectively functionalizing the nanorod tips with polystyrene while leaving the CTAB bilayer along the sides of the NRs largely intact. Interestingly, the conformations of the polymers on the nanorod tips were shown to strongly influence the assembled nanorod chains, which may allow for tuning of nanorod assemblies by controlling grafting density, solvent quality, or the stiffness of the polymer backbone.[13] While solution NMR measurements can be difficult for large nanoparticles (>2 nm),[14] solid state NMR measurements of ZnSe[15] and CdSe nanocrystals[16] have been successful in quantifying the adsorption of capping molecules after synthesis. For Au NRs, which can be over 100 nm in length, complementary techniques are necessary.

Small-angle neutron scattering (SANS) is an ideal tool for studying Au NRs due to its isotopic sensitivity. In particular, SANS can directly probe the structure and composition of the Au core, surfactant bilayer, and polymer layer which is challenging using electron microscopy or X-ray techniques alone. To the best of our knowledge, only a single study from Gómez-Graña and co-workers has examined Au NRs using SANS.[17] In fact, Gómez-Graña et al. used a combination of small-angle X-ray scattering (SAXS) and SANS to confirm the presence of a CTAB bilayer along the surface of Au NRs. The thickness of this bilayer was found to be 3.4 nm, slightly thinner than expected based on the length of individual CTAB molecules. Thus, the study concluded that some degree of interdigitation of the surfactant molecules must occur. The authors also noted, however, that significantly higher concentrations of Au NRs are needed to probe the surface coatings of Au NRs in greater detail. A further challenge in interpreting SANS measurements lies in the difficulty in determining the Au NR volume fraction in solution, since the molar extinction coefficient for Au NRs depends on their dimensions. While calculations using the discrete dipole approximation (DDA) have proven useful, work from Near et al. finds that extinction coefficients determined from DDA must be multiplied by a conversion factor in order to be mapped onto experimental systems.[18]

Though several examples in the literature clearly demonstrate the importance of the Au NR surface coating for applications, no detailed characterization of the composition and location exists, likely due, in part, to the difficulty in obtaining high concentrations of low polydispersity Au NRs for scattering experiments. Here, we report neutron scattering measurements of surfactant- or polymer-coated Au NRs to address three important questions. First, we show that the structure of the surfactant bilayer on Au NRs is not affected by the use of CTAC in the synthesis process, recovering scattering results that are in quantitative agreement with scattering from CTAB-coated Au NRs. Second, through selective deuteration of surfactant on the seed crystals from which the Au NRs are grown, we demonstrate that almost all of the initial surface coating is transferred to the final NRs, and moreover, that even after 30 days between synthesis and SANS measurements, almost no exchange of surfactant between the bilayer and solution occurs, which could potentially lead to novel methods of incorporating small molecules into NRs and their assemblies. Finally, we characterize the surfaces of Au NRs after they are functionalized with a thiol-terminated polymer. Interestingly, we observe that, upon functionalizing Au NRs with thiol-terminated poly(ethylene glycol), the SANS pattern remains qualitatively similar to that of the surfactant-coated NRs, indicating that the polymer does not completely displace the surfactant molecules, which may be a critical consideration when using Au NRs in biological applications.

Results and Discussion. In the following sections, surfactant and polymer-grafted Au NRs will be characterized by SANS to understand the structure, location, and composition of the surface layers. Au NR samples were labeled

DOI: 10.1021/acs.nanolett.5b03088
Nano Lett. 2015, 15, 5730−5738

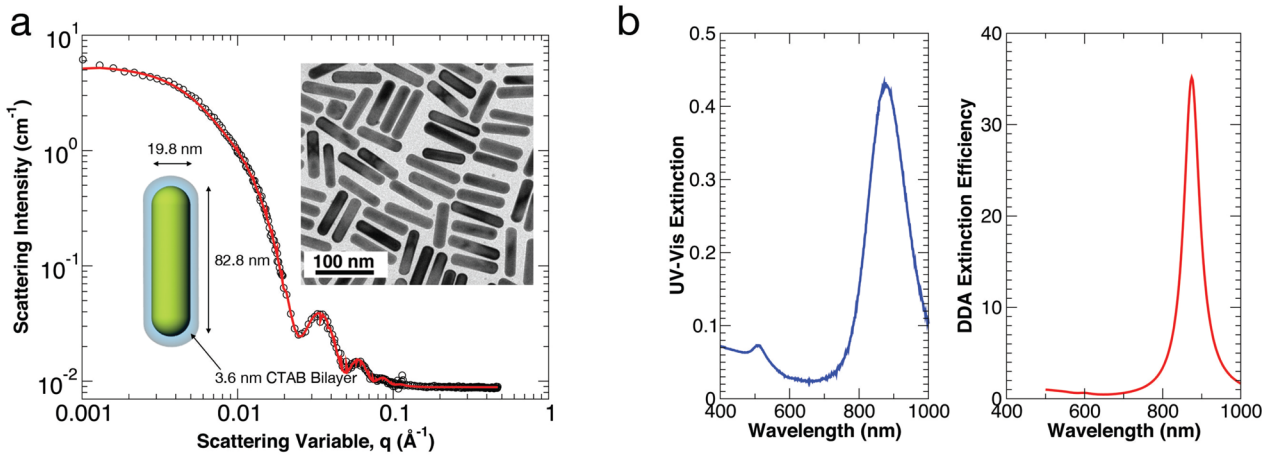

Figure 1. (a) Small-angle neutron scattering data from sample $hCTAB_1$ in D_2O. The red line is the least-squares fit to the data (open circles) using a core−shell cylinder model. The inset transmission electron microscopy (TEM) image demonstrates low polydispersity Au NRs with diameters of approximately 20 nm, and lengths of approximately 83 nm. The scale bar is 100 nm. (b) UV−vis (left) and discrete dipole approximation (DDA) calculation (right) of the extinction and extinction efficiency, respectively, for sample $hCTAB_1$. The peak near 880 nm corresponds to the longitudinal surface plasmon resonance (LSPR).

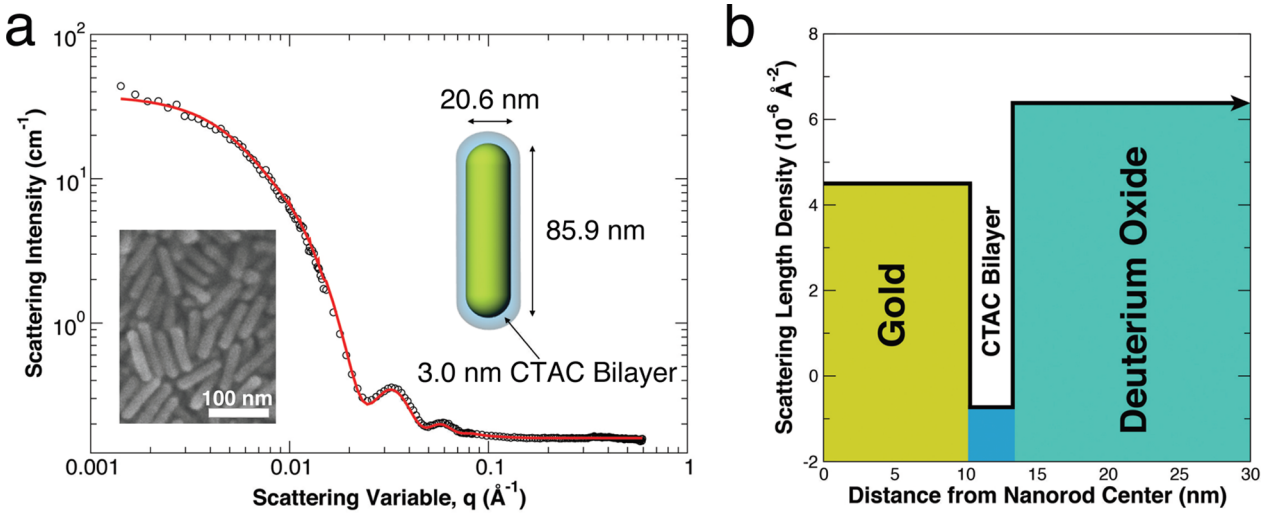

Figure 2. (a) Small-angle neutron scattering data from sample $hCTAC_1$ in D_2O. The red line is a least-squares fit to the scattering data using a core−shell cylinder model. The best fit line indicates that the Au NRs are 20.6 nm in diameter and 85.9 nm in length. A 3.0 nm shell is observed, consistent with the presence of a surfactant bilayer. The inset is an electron micrograph of the Au NRs deposited on silicon. (b) Scattering length densities (SLDs) of the core, shell, and solvent. The SLD of the surfactant bilayer is -7.3×10^{-7} Å^{-2}, identical to that of CTAB.

according to the isotope of hydrogen present in the seed crystal surfactant, the surfactant used in the growth solution, and a sample ID. For instance, sample $hCTAB_1$ contained hydrogenated CTAB in the seed solution (h), CTAB in the growth solution, and is the first sample of the series. Similarly, sample $dCTAC_1$ contained deuterated CTAB in the seed solution (d), CTAC in the growth solution, and is the first sample of the series. The characterization of the Au NR samples, along with the calculated molar extinction coefficients, is summarized in Table 1. Because synthesis of Au NRs in the presence of CTAC is not as common in the literature, we have provided the UV−vis spectra for all samples in the Supporting Information.

Surfactant Coated Au NRs. Because neutrons interact primarily with the atomic nucleus, the scattered intensity depends strongly on the isotopes present in the sample. In Figure 1, (a) SANS from sample $hCTAB_1$ is shown, along with a representative TEM image and (b) optical extinction data. The SANS data is fit using an orientationally averaged core−shell cylinder model (equation S2, Supporting Information). We take the shell thickness along the radial and length directions to be the same, $t = t_R = t_L$, which yields the dimensions of the core and a uniform shell, as well as the Au NR volume fraction in solution. The best fit yields a core radius of $R_{NR} = 9.9$ nm, a core length of $L_{NR} = 82.8$ nm, and a CTAB shell thickness of $t = 3.6$ nm, which is in quantitative agreement with a previous study from Gómez-Graña et al., who measured $t \approx 3.4$ nm.[17] Note that, while the core dimensions obtained from SANS are in agreement with those obtained from the TEM image in the inset of Figure 1a, the shell thickness cannot be obtained from TEM. From UV−vis measurements, the calculated Au NR volume fraction in sample $hCTAB_1$ is 5.85×10^{-5}, which is in reasonable agreement with the fitted SANS data: $\varphi = 5.37 \pm 0.06 \times 10^{-5}$. Using the volume fraction determined from UV−vis, fits to the scattering intensity yield a CTAB scattering length density (SLD) of $-7.3 \pm 0.5 \times 10^{-7}$ Å^{-2}, in good agreement with the expected value. Thus, the

DOI: 10.1021/acs.nanolett.5b03088
Nano Lett. 2015, 15, 5730−5738

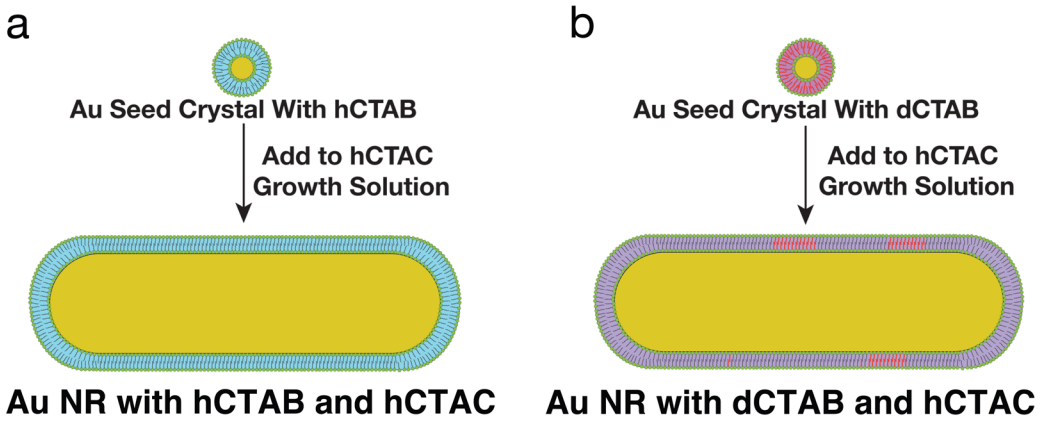

Figure 3. Schematic illustrating the detection of surfactant transfer from the seed crystal to the final nanorod through selective deuteration of CTAB on the seed crystal. (a) Using hydrogenated CTAB (hCTAB) on the seed crystal leads to a surfactant layer that is a mixture of hCTAB and hydrogenated CTAC (hCTAC). Due to the identical chemical structure of the surfactant, no change in the scattering length density (SLD) of the final surface coating is measured. (b) Since deuterated CTAB (dCTAB) has a significantly higher SLD than hydrogenated CTAB or hydrogenated CTAC, the bilayer on the synthesized Au NR has an effective SLD that is between $\rho = -7.3 \times 10^{-7}$ Å^{-2} and $\rho = 7.06 \times 10^{-6}$ Å^{-2}.

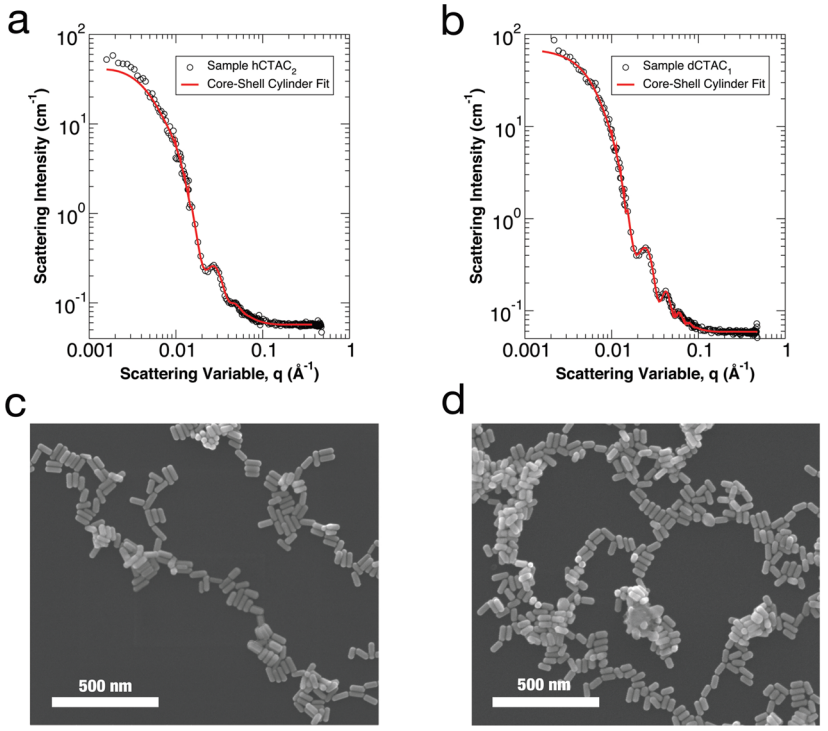

Figure 4. Small-angle neutron scattering and scanning electron micrographs (SEM) from Au NRs prepared using a seed solution with hydrogenated CTAB ($hCTAC_2$: a, c) and deuterated CTAB ($dCTAC_1$: b, d). SEM images demonstrate that the NRs are similar in size, whereas SANS indicates a larger value of the SLD for the surfactant bilayer, implying that dCTAB remains on the Au NR surface after synthesis.

combination of electron microscopy, SANS, and UV−vis measurements is able to completely characterize the dimensions of the Au NR core and surfactant shell. However, while EDS measurements by others[7] can resolve the very thin layer of Ag atoms along the Au NR surface, SANS cannot resolve such features or provide additional information regarding its role in the synthesis of Au NRs.

CTAC-coated Au NRs were synthesized according to a method from Ye et al.,[4] in the presence of CTAC, silver ions, sodium oleate (NaOL), gold ions, and small, CTAB-coated Au seed crystals (see Supporting Information). CTAB and CTAC differ only in their halide counterion, bromide or chloride, respectively. Therefore, scattering from hydrogenated CTAB and CTAC is expected to produce the same scattering length density for the hydrophobic tail: -7.3×10^{-7} Å^{-2}. NaOL, on the other hand, has a scattering length density that is on the order of 10^{-8} Å^{-2}, meaning that its presence cannot be detected within the uncertainty of our SANS measurements. Nevertheless, on the basis of the similarities in the surfactant bilayer thicknesses measured by us in the presence of NaOL (cf. Figure 1) and by Gómez-Graña et al.[17] in the absence of NaOL, we do not believe that NaOL strongly influences the structural characteristics of the surfactant layers and neglect it in our analysis.

DOI: 10.1021/acs.nanolett.5b03088
Nano Lett. 2015, 15, 5730−5738

In Figure 2, (a) SANS data is shown for sample $hCTAC_1$ along with (b) the scattering length densities determined from the least-squares fit. The core−shell cylinder model finds that the Au NRs have an average diameter of 20.6 nm and average length of 85.9 nm. The thickness of the CTAC layer is 3.0 nm, indicating that the bilayer on Au NRs grown with CTAC is similar to that on NRs grown in CTAB solutions, except slightly thinner. The volume fraction of NRs in sample $hCTAC_1$ was $\varphi \approx 4.17\times 10^{-4}$, with a CTAC SLD of $-7.31 \pm 0.02 \times 10^{-7}$ Å^{-2}. Despite the influence of CTAC on the crystalline structure of the final Au NR product, the structure of the bilayer is not significantly altered due to different possible adsorption characteristics of the surfactant molecules (i.e., CTAC versus CTAB).

To determine the amount of CTAB that is transferred from the CTAB-coated seed crystals to the CTAC-coated Au NRs, a Au seed was synthesized using deuterated CTAB (dCTAB) rather than the usual hydrogenated CTAB (hCTAB). These seeds were then injected into a growth solution containing hydrogenated CTAC. Note that the SLD for dCTAB ($\rho_{dCTAB} \approx 7.06 \times 10^{-6}$ Å^{-2}) is an order of magnitude larger than hCTAB ($\rho_{hCTAB} = -7.3 \times 10^{-7}$ Å^{-2}), and opposite in sign. Thus, the presence of dCTAB in a hydrogenated CTAC bilayer serves to increase the measured scattering length density of the shell, as illustrated schematically in Figure 3. As shown in Figure 4a, by using the known Au NR dimensions determined from SEM (Figure 4c) and known scattering length densities of gold, D_2O, and CTAC, the scattering intensity is well-described by a core−shell cylinder model, yielding a volume fraction of NRs of approximately $\varphi \approx 4.6 \pm 0.1 \times 10^{-4}$, which is again consistent with estimations from UV−vis. The best fit to sample $dCTAC_1$ (Figure 4b and d), which was prepared using a seed solution with deuterated CTAB, shows an increased scattering length density in the surfactant shell of $-3.0 \pm 0.7 \times 10^{-7}$ Å^{-2}. Using a linear mixing rule, this corresponds to a mole fraction of approximately 5% deuterated CTAB in the bilayer. The presence of even small amounts of polydispersity in the nanorod dimensions will affect the SLD obtained from SANS; thus, the value of $\rho \approx -3.0 \times 10^{-7}$ Å^{-7} repesents an average across the sample. Nevertheless, SANS clearly demonstrates that a measurable amount of surfactant from the seed solution remains within the bilayer of the final Au NR product. While the NRs in Figure 4c and d appear aggregated, this is the result of drying effects during sample preparation. The lack of a power law behavior in the scattering at low q (cf., Figure 4a and b) shows that the Au NRs disperse completely in solution.

The presence of 5% mole fraction of dCTAB in the hCTAC bilayer implies that minimal surfactant exchange occurs between the Au seed crystals and the growth solution. This can be realized by assuming a roughly uniform coating of the CTAB bilayer on the Au seed crystals. The volume of a surfactant molecule is $v \approx (27.4 + 26.9n) \times 10^{-3}$ nm^3,[19] where n is the number of carbons along the hydrocarbon chain. Thus, for a chain of 16 carbon atoms, $v \approx 0.458$ nm^3. For typical 3 nm Au seed crystals, approximately 1045 CTAB molecules are needed to form a bilayer around the gold core. After growth in a CTAC solution, Au NRs that are 15.3 nm × 83.4 nm would be coated in approximately 57271 surfactant molecules. Thus, if all of the 1045 deuterated CTAB molecules are present in the final surfactant bilayer, approximately 2% of the molecules would be deuterated, which is on the order of the value measured experimentally (5%). Because of the curvature of the nanoparticle surface, the number of surfactant molecules in the outer leaflet is different than that in the inner leaflet, near the surface. For this reason, the volume of the bilayer must be used in this calculation instead of the surface area. However, as the surface area of the nanorod increases, the corresponding SLD of the surfactant shell should approach that of pure hCTAB/hCTAC due to an increasing majority of hydrogenated surfactant species. To test this hypothesis, we performed SANS measurements on four additional Au NR samples with various dimensions. Sample $dTSAC_1$ was prepared with trimethylstearylammonium chloride (TSAC, $C_{21}H_{46}NCl$) in place of CTAC to also determine whether a longer surfactant chain causes a measurable increase in the surfactant bilayer thickness. TSAC has two additional carbons in the main chain of the molecule as compared to CTAB or CTAC.

The SANS measurements and fits to the scattered intensity are presented in Figure 5a. Interestingly, the measurements show that the thickness of the surfactant layer in the deuterated samples is approximately 2.5−2.8 nm, considerably lower than the nominal value of 3.4 to 3.6 nm that has been measured both by us and by Gómez-Graña et al.[17] While the origin of this difference is unknown, it may be due a number of factors such as the age of the NRs (Au NRs were stored for more than 30 days in pure Milli-Q water when measured), the presence of Cl^- instead of Br^-, or an effect of the deuterated surfactant. In addition, the thickness of the TSAC layer is found to be close to that of the CTAC layer, despite the slightly longer hydrocarbon chains, which suggests interdigitation of the leaflets of the bilayer.

As predicted by the crude space filling model above, the SLD of the surfactant shell decreases as the dimensions (characterized by the surface area) increase. In Figure 5b, the measured SLD of the surfactant shell is plotted as a function of nanorod surface area. The SLD of the deuterated samples (squares) decreases and eventually saturates at the SLD of hCTAC as the surface area increases (triangles). The blue dotted line shows the predicted value of the SLD from the space filling model described above. While the theoretical values do not agree quantitatively with those measured using SANS, it is worth noting that the space filling model is only approximate and does not take into account packing densities in the bilayer. In addition, free deuterated surfactant may be introduced into the hydrogenated CTAC growth solution when the seed crystals are injected, which may slightly increase the amount of deuterated surfactant present relative to our model. However, this would account for less than 1% of the deuterated surfactant and should be a negligible effect. Nevertheless, this simple model qualitatively reproduces the trends observed experimentally. A significant result of these measurements is the demonstration of the retention of a substantial amount of deuterated surfactant from the seed crystals to the final NRs, which might be exploited in future studies to incorporate small molecules, for example, into the surfactant layers during the synthesis process.

Polymer Grafted Au NRs. For many applications, including those in which Au NRs are introduced into the body, the cytotoxic CTAB should be replaced by a more benign molecule. In addition, to create a stable dispersion of Au NRs in a polymer matrix, the surfactant must normally be replaced by polymer chains that are compatible with the matrix polymers.[9] This replacement is performed using thiol-terminated polymers, which are thought to displace the surfactant molecules due to the strong binding affinity of -SH to gold surfaces. While neutron scattering techniques are able

DOI: 10.1021/acs.nanolett.5b03088
Nano Lett. 2015, 15, 5730−5738

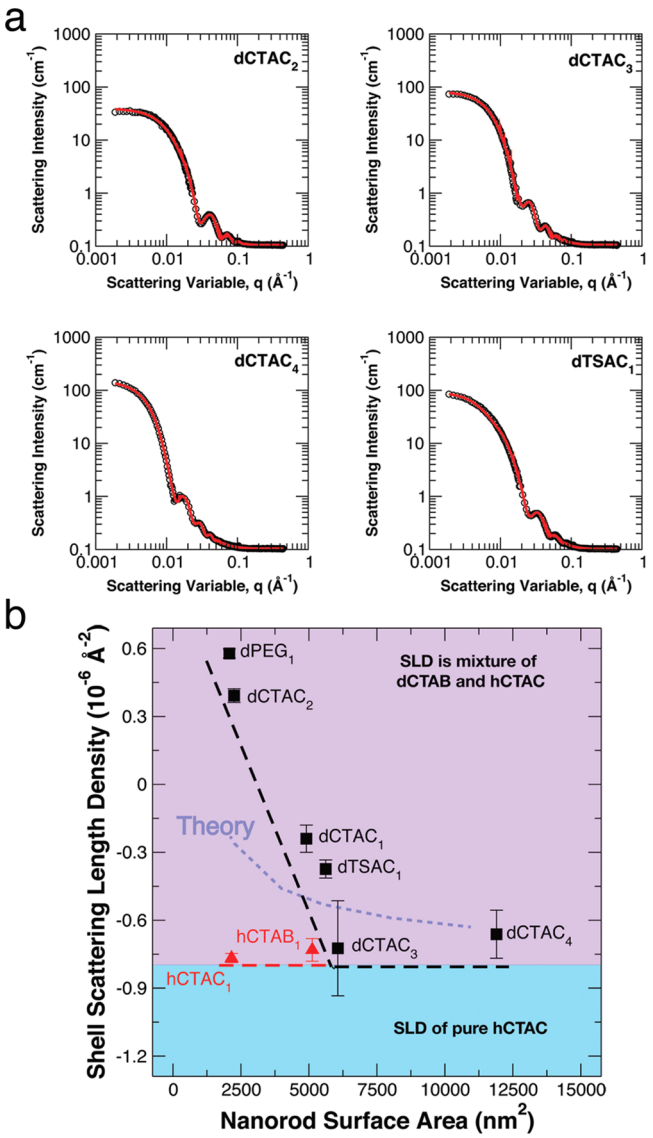

Figure 5. (a) Small-angle neutron scattering measurements for samples $dCTAC_2$–$dCTAC_4$ and $dTSAC_1$. The black points are data, and the red lines are fits according to a core–shell cylinder model. (b) The scattering length density (SLD) of the surfactant shell extracted from fits to SANS data is plotted as a function of nanorod surface area for Au NRs synthesized from seed crystals with deuterated surfactant (black) and hydrogenated surfactant (red). For large values of surface area, the SLD of the deuterated samples approach that of pure hCTAC/hCTAB, whereas for smaller values, the SLD is higher because a larger mole fraction of deuterated molecules is retained on the Au NR surface. The dotted line is the theoretical prediction for the SLD variation based upon a model that assumes uniform packing of surfactant molecules around the nanoparticles.The dashed lines are guides for the eye. Error bars on the SLD values correspond to one standard deviation in the least-squares fit.

to directly resolve the polymer thickness and chain conformation, the structure of polymer coatings on Au NRs has only been studied experimentally using electron microscopy.

Polymers that are grafted to nanoparticle surfaces adopt a range of conformations. At low grafting densities, in the "mushroom" regime, the chains do not feel the presence of neighboring chains and adopt ideal, Gaussian conformations with an average radius of gyration that scales as $R_g \sim N^{0.5}$, where N is the degree of polymerization of the chain. As the grafting density increases, chains become increasingly confined by other chains in their vicinity and start to exhibit larger values of R_g in the semidilute polymer brush (SDPB) regime. At very high grafting densities, grafted polymers exhibit two primary scaling relations. Near the surface of the nanoparticle, up to a cutoff distance r_c, the chains are highly stretched with a thickness that scales as $N^{0.8}$ in the concentrated polymer brush (CPB) regime.[20,21] The value of r_c depends principally on the nanoparticle radius and polymer grafting density and can be obtained by extending the classical Daoud–Cotton model to a curved surface.[20,22] At distances larger than r_c, the polymer chains transition to the SDPB regime and adopt a Gaussian conformation in a melt or a swollen conformation in a good solvent. These predictions have been confirmed for spherical particles using electron microscopy,[23,24] dynamic light scattering,[20,21] and most recently, small-angle neutron scattering.[25]

The photographs in Figure 6a show solutions of Au NRs in water, methanol, and toluene before (top) and after (bottom) functionalization with SH-PEG. Before functionalization, CTAC-coated Au NRs disperse in water, whereas they fall out of solution when the solvent is exchanged with methanol (middle) or toluene (right). On the other hand, the same Au NRs disperse in water, methanol, and toluene once functionalized with SH-PEG, confirming the presence of PEG on the nanorod surface. Thermogravimetric analysis from previous studies has found the grafting density of 5 kg/mol SH-PEG to be approximately $\sigma = 0.5$ nm^{-2}.[26,27] On the basis of the extended Daoud–Cotton model (equation S7, Supporting Information), we estimate that for $\sigma = 0.5$ nm^{-2}, $r_c \approx 30$–35 nm. Thus, using the Kuhn length ($b = 1.1$ nm) and Kuhn molar mass ($M_0 = 137$ g/mol) for SH-PEG ($M_n = 5$ kg/mol), the thickness of the surface layer should be approximately $t_{PEG} = 18$–19 nm, meaning the entirety of the SH-PEG chain should be in the CPB regime and highly stretched.[28,29]

SANS scattering data are shown in Figure 6b for PEG-functionalized Au NRs (sample $dPEG_1$, circles). The scattering for $dPEG_1$ contains many oscillations in the data as indicated by the black arrows, which is characteristic of scattering from an object with a uniform density. The data are fit using a modified core–shell cylinder function that also accounts for the presence of SH-PEG chains (equation S4, Supporting Information). The best fit to the scattering intensity (solid red line) reveals a Au core that is approximately 16 nm in diameter and 41 nm in length. Surrounding the Au core is a layer of uniform density molecules with a thickness of approximately 3.5 nm, which is an order of magnitude less than the predicted value of t_{PEG}. The SLD measured is on the order of that expected for PEG ($\rho_{PEG} \approx 5 \times 10^{-7}$ Å^{-2}),[30] but this value of the SLD is also close to that expected if no SH-PEG were present at all (cf., Figure 5b). The SH-PEG chains have an average radius of gyration of 3.1 nm and a grafting density $\sigma \approx 0.002 \pm 0.0005$ chains/nm^2. Using the Kuhn length and Kuhn mass, the 5 kg/mol SH-PEG chains are estimated to have an average radius of gyration of 2.7 nm, indicating the SH-PEG chains on the nanorod are slightly stretched. Note that although R_g for the SH-PEG chains is on the order of the surfactant thickness, scattering from the fractal SH-PEG chains has a distinct shape compared to that of the surfactant bilayer, making it possible to estimate the amount of SH-PEG present. Specifically, scattering from SH-PEG increases the scattering intensity and simultaneously smears out the oscillatory features due to the Au core and surfactant bilayer. For comparison, the scattering data for sample

DOI: 10.1021/acs.nanolett.5b03088
Nano Lett. 2015, 15, 5730–5738

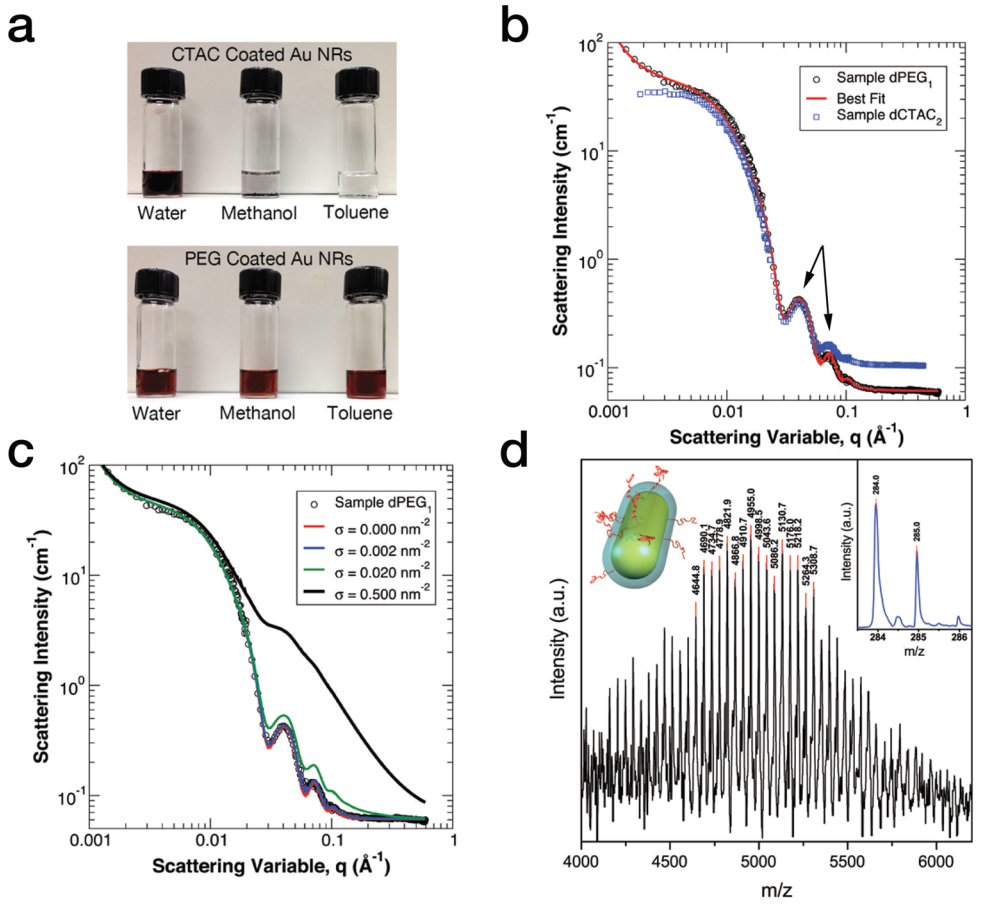

Figure 6. (a) Photographs of CTAC (top) and PEG coated Au NRs (bottom) in water (left), methanol (middle), and toluene (right). The CTAC coated Au NRs only disperse in water, whereas the PEG coated Au NRs disperse in all three solvents, indicating the presence of PEG on the surface. (b) SANS measurements (circles) and best fit (line) for $dPEG_1$ in D_2O. The fit yields a SH-PEG grafting density of σ = 0.002 chains/nm^2. For comparison, sample $dCTAC_2$ is overlaid (squares) The arrows highlight oscillations due to a uniform core−shell structure. (c) SANS measurements of $dPEG_1$ with models assuming SH-PEG grafting densities of σ = 0.000 chains/nm^2 (red), σ = 0.002 chains/nm^2 (blue, best fit), σ = 0.020 chains/nm^2 (green), and σ = 0.500 chains/nm^2 (black). (d) MALDI-TOF spectrum of $dPEG_1$ after ligand exchange and extraction, showing that the SH-PEG is present on the nanorod. Inset shows a NALDI-TOF spectrum of $dPEG_1$, indicating CTAC is also present on the nanorod. The cartoon schematic shows the assumed structure of the NRs in $dPEG_1$ on the basis of the data in a−c. The red curves are PEG chains, and the blue halo is the CTAC bilayer.

$dCTAC_2$, which has similar dimensions to $dPEG_1$, are overlaid on the scattering from sample $dPEG_1$. The two sets of data coincide, and the oscillations occur at the same values of the scattering variable q, implying that the overall structure and thickness of the surface layer is identical between the two samples. The difference in the scattering intensity for large values of q is due to a difference in the scattering background.

If the Au NRs were predominantly grafted with SH-PEG, the shape of the scattering curve would appear different than that in Figure 6b. Most notably, because of scattering from the fractal-like SH-PEG chains, the oscillations would be largely absent, and the scattering in this region would be described by a smooth decay in intensity[25] to the background (B) as $I(q) \sim q^{-2} + B$—a behavior which is not observed in our measurements. For this reason, the data strongly indicate that the surfactant bilayer remains almost entirely intact after PEGylation of the Au NRs. This can be observed in Figure 6c, where the scattering data are fit with different grafting densities of SH-PEG. For low grafting densities of σ = 0.00 (red) and σ = 0.002 chains/nm^2 (blue), the model fits the data well, with σ = 0.002 ± 0.0005 chains/nm^2 representing the best fit to the data. This value of the grafting density corresponds to approximately 6 SH-PEG chains per Au NR. While this value may appear exceedingly small, work from Jiao and Akcora[31] has shown that such low grafting densities are sufficient for processing polymer-grafted nanoparticles. Fits using a higher grafting density of σ = 0.02 chains/nm^2 have a high intensity in the oscillatory region of the scattering data. Also shown in black in Figure 6c is a fit for σ = 0.50 chains/nm^2, which corresponds to the grafting density indicated by thermogravimetric analysis (TGA). Interestingly, neither of these curves accurately describe the scattering data, with σ = 0.50 chains/nm^2 exhibiting the smooth decay in the scattering intensity that is expected from scattering from a large quantity of polymer chains. Thus, the shape and intensity of the scattering data point toward Au NRs that are predominantly coated in surfactant after PEGylation.

Because the fits to the SANS data indicate a very low SH-PEG grafting density, mass spectrometry measurements were performed to determine if the presence of SH-PEG could be verified using complementary techniques. The presence of both the cetyltrimethylammonium cation (CTA^+) and SH-PEG is confirmed by the mass spectrometry data shown in Figure 6d. Matrix-assisted and nanostructure-assisted laser desorption/

DOI: 10.1021/acs.nanolett.5b03088
Nano Lett. 2015, 15, 5730−5738

ionization time-of-flight (MALDI-TOF and NALDI-TOF, respectively) mass spectrometry clearly resolves the presence of 5 kg/mol SH-PEG (m/z = 4500−5000), as well as the CTA^+ cation (inset) for m/z = 284 and 285. However, these mass spectrometry measurements are unable to determine the relative amounts of CTA^+ and SH-PEG that are present in the bilayer that surrounds the Au NRs.

The presence of residual capping agents, such as surfactant, after functionalization of nanoparticles with polymers has been previously documented in the literature. Recent work from the Mefford group[32] using ^{14}C-labeled oleic acid has quantitatively determined that surface coatings on nanospheres remain in place after grafting-to functionalization with polymers—even at high polymer grafting densities. In the case of Au NRs, X-ray photoelectron spectroscopy (XPS) measurements[33] of Au NRs after an identical PEGylation procedure as used here determined that the elemental percentage of bromine decreased from 7% to 0.8% upon grafting the NRs with 5 kg/mol SH-PEG, indicating the replacement of the majority of CTAB with SH-PEG. Energy-dispersive X-ray spectroscopy (EDS) measurements (Figure S3, Supporting Information) of sample $dPEG_1$ detect the presence of the chloride counterion, which is consistent with previous XPS measurements.

While our EDS measurements are in qualitative agreement with previous XPS measurements,[33] the combination of SANS with MALDI-TOF demonstrates that substantially more surfactant remains adsorbed to the surface after functionalization than previously thought and that EDS and XPS may not be appropriate techniques to assess the composition of the surface layers on Au NRs. The SANS measurements in Figure 6b and d quantitatively show that the 3.5 nm surfactant bilayer on the nanorod surface is not altered or disrupted by the presence of a small amount of SH-PEG, which must be taken into consideration when using Au NRs in biological systems or when determining polymer grafting density using thermogravimetric analysis (TGA).

Summary. In summary, we have performed extensive small-angle neutron scattering (SANS) measurements of Au NRs that have either adsorbed bilayers of surfactant or that are grafted with thiol-terminated poly(ethylene glycol). Measurements of surfactant-coated Au NRs show a surfactant layer with thicknesses between approximately 2.5 and 3.7 nm, with those samples which contain CTAC having a lower thickness (t < 3.0 nm) than those prepared with CTAB. The nanorod dimensions measured with SANS are in excellent quantitative agreement with those measured from electron micrographs.

By selectively deuterating the surfactant present on the surfaces of seed crystals, we directly measured the amount of surfactant that is retained on the Au surface during nanorod synthesis. Interestingly, we find that almost all of the original surfactant is retained on the surface, which implies minimal exchange between the nanoparticle coating and solution. This fact might be exploited in future work to incorporate small molecules into the surfactant coating, since the synthesis of Au seed crystals may not be as sensitive to synthesis conditions as the synthesis of Au NRs and represents a relatively unexplored area of Au NR synthesis.

Finally, we have quantitatively demonstrated that, when Au NRs are functionalized with a thiol-terminated polymer under aqueous conditions, the ≈3 nm surfactant coating remains and is not significantly disrupted. Although a small amount of polymer is present which facilitates dissolving the Au NRs in organic solvents or dispersing within a polymer matrix, the presence of a thick surfactant layer, confirmed via mass spectrometry and EDS measurements, should be taken into account in future TGA measurements of polymer grafting density. In addition, because CTAB/CTAC is cytotoxic, this residual surfactant may have unanticipated consequences when PEG-grafted Au NRs are used in biological applications. For applications that are sensitive to nanoparticle separation, such as in plasmonic devices, the residual surfactant layer may place physical constrains on the interparticle separations that are achievable in the lab. Future work should address the implications of the residual surfactant layer and seek opportunities to access surfactant-free, high grafting density layers of polymers on Au NRs.

■ ASSOCIATED CONTENT

Supporting Information

The Supporting Information is available free of charge on the ACS Publications website at DOI: 10.1021/acs.nanolett.5b03088.

Experimental procedures, small-angle neutron scattering model, extended Daoud−Cotton model, UV−vis, EDS, and MALDI-TOF mass spectrometry measurements (PDF)

■ AUTHOR INFORMATION

Corresponding Author

*E-mail: hore@case.edu.

Present Address

X.Y.: Department of Chemistry, University of California Berkeley, Berkeley CA, USA.

Notes

The authors declare no competing financial interest.

■ ACKNOWLEDGMENTS

The identification of commercial products or experimental methods does not imply endorsement by the National Institute of Standards and Technology nor does it imply that these are the best for the purpose. This work utilized neutron scattering facilities supported in part by the National Science Foundation (NSF) under Agreement No. DMR-0944772. M.J.A.H. acknowledges support from a National Research Council (NRC) postdoctoral associateship at the NIST Center for Neutron Research (NCNR) during a portion of this research. R.J.C. acknowledges funding from NSF Polymer (DMR-0907493) and MRSEC (DMR-1120901) programs. X.Y., Y.G., J.F., and C.B.M. acknowledge support from the Office of Naval Research (ONR) Multidisciplinary University Research Initiative (MURI) on Optical Metamaterials through award N00014-10-1-0942. C.B.M. is also grateful to the Richard Perry University Professorship for support of his supervisor role.

■ REFERENCES

(1) Lohse, S. E.; Murphy, C. J. *Chem. Mater.* **2013**, *25*, 1250−1261.

(2) Ye, X.; Jin, L.; Caglayan, H.; Chen, J.; Xing, G.; Zheng, C.; Doan-Nguyen, V.; Kang, Y.; Engheta, N.; Kagan, C. R.; Murray, C. B. *ACS Nano* **2012**, *6*, 2804−2817.

(3) Ye, X.; Zheng, C.; Chen, J.; Gao, Y.; Murray, C. B. *Nano Lett.* **2013**, *13*, 765−771.

(4) Ye, X.; Gao, Y.; Chen, J.; Reifsnyder, D. C.; Zheng, C.; Murray, C. B. *Nano Lett.* **2013**, *13*, 2163−2171.

DOI: 10.1021/acs.nanolett.5b03088
Nano Lett. 2015, 15, 5730−5738

(5) Carbó-Argibay, E.; Rodríguez-González, B.; Gómez-Graña, S.; Guerrero-Martínez, A.; Pastoriza-Santos, I.; Pérez-Juste, J.; Liz-Marzán, L. M. *Angew. Chem.* **2010**, *122*, 9587−9590.
(6) Park, K.; Drummy, L. F.; Wadams, R. C.; Koerner, H.; Nepal, D.; Fabris, L.; Vaia, R. A. *Chem. Mater.* **2013**, *25*, 555−563.
(7) Jackson, S. R.; McBride, J. R.; Rosenthal, S. J.; Wright, D. W. *J. Am. Chem. Soc.* **2014**, *136*, 5261−5263.
(8) Pierrat, S.; Zins, I.; Breivogel, A.; Sönnichsen, C. *Nano Lett.* **2007**, *7*, 259−263.
(9) Hore, M. J. A.; Composto, R. J. *Macromolecules* **2014**, *47*, 875−887.
(10) Dubois, L. H.; Nuzzo, R. G. *Annu. Rev. Phys. Chem.* **1992**, *43*, 437−463.
(11) Vigderman, L.; Manna, P.; Zubarev, E. R. *Angew. Chem.* **2012**, *124*, 660−665.
(12) Nie, Z.; Fava, D.; Kumacheva, E.; Zou, S.; Walker, G. C.; Rubinstein, M. *Nat. Mater.* **2007**, *6*, 609−614.
(13) Nie, Z.; Fava, D.; Rubinstein, M.; Kumacheva, E. *J. Am. Chem. Soc.* **2008**, *130*, 3683−3689.
(14) Abraham, A.; Mihaliuk, E.; Kumar, B.; Legleiter, J.; Gullion, T. *J. Phys. Chem. C* **2010**, *114*, 18109−018114.
(15) Berrettini, M. G.; Braun, G.; Hu, J. G.; Strouse, G. F. *J. Am. Chem. Soc.* **2004**, *126*, 7063−7070.
(16) Cadars, S.; Smith, B. J.; Epping, J. D.; Acharya, S.; Belman, N.; Golan, Y.; Chmelka, B. F. *Phys. Rev. Lett.* **2009**, *103*, 136802.
(17) Gómez-Graña, S.; Hubert, F.; Testard, F.; Guerrero-Martínez, A.; Grillo, I.; Liz-Marzán, L. M.; Spalla, O. *Langmuir* **2012**, *28*, 1453−1459.
(18) Near, R. D.; Hayden, S. C.; Hunter, R. E., Jr.; Thackston, D.; El-Sayed, M. A. *J. Phys. Chem. C* **2013**, *117*, 23950−23955.
(19) Israelachvili, J. N. *Forces Intermolecular and Surface*, 2nd ed.; Academic Press: Burlington, MA, 1991.
(20) Ohno, K.; Morinaga, T.; Takeno, S.; Tsujii, Y.; Fukuda, T. *Macromolecules* **2007**, *40*, 9143−9150.
(21) Dukes, D.; Li, Y.; Lewis, S.; Benicewicz, B.; Schadler, L.; Kumar, S. K. *Macromolecules* **2010**, *43*, 1564−1570.
(22) Daoud, M.; Cotton, J. P. *J. Phys. (Paris)* **1982**, *43*, 531−538.
(23) Choi, J.; Dong, H.; Matyjaszewski, K.; Bockstaller, M. R. *J. Am. Chem. Soc.* **2010**, *132*, 12537−12539.
(24) Choi, J.; Hui, C. M.; Schmitt, M.; Pietrasik, J.; Margel, S.; Matyjazsewski, K.; Bockstaller, M. R. *Langmuir* **2013**, *29*, 6452−6459.
(25) Hore, M. J. A.; Ford, J.; Ohno, K.; Composto, R. J.; Hammouda, B. *Macromolecules* **2013**, *46*, 9341−9348.
(26) Deshmukh, R. D.; Liu, Y.; Composto, R. J. *Nano Lett.* **2007**, *7*, 3662−3668.
(27) Hore, M. J. A.; Composto, R. J. *ACS Nano* **2010**, *4*, 6941−6949.
(28) Saffer, E. M.; Lackey, M. A.; Griffin, D. M.; Kishore, S.; Tew, G. N.; Bhatia, S. R. *Soft Matter* **2014**, *10*, 1905−1916.
(29) Rubenstein, M.; Colby, R. H. *Polymer Physics*, 1st ed.; Oxford University Press: Oxford, 2003.
(30) Zeroni, I.; Lodge, T. P. *Macromolecules* **2008**, *41*, 1050−1052.
(31) Jiao, Y.; Akcora, P. *Macromolecules* **2012**, *45*, 3463−3470.
(32) Davis, K.; Qi, B.; Witmer, M.; Kitchens, C. L.; Powell, B. A.; Mefford, O. T. *Langmuir* **2014**, *30*, 10918−10925.
(33) Thierry, B.; Ng, J.; Krieg, T.; Griesser, H. J. *Chem. Commun.* **2009**, 1724−1726.

DOI: 10.1021/acs.nanolett.5b03088
Nano Lett. 2015, 15, 5730−5738